Human Molecular Genetics, 2017, Vol. 26, No. 24 4861–4872

doi: 10.1093/hmg/ddx364
Advance Access Publication Date: 25 September 2017
Original Article

ORIGINAL ARTICLE

Progranulin-mediated deficiency of cathepsin D results in FTD and NCL-like phenotypes in neurons derived from FTD patients

Clarissa Valdez[1], Yvette C. Wong[1], Michael Schwake[1], Guojun Bu[2], Zbigniew K. Wszolek[3] and Dimitri Krainc[1,*]

[1]The Ken & Ruth Davee Department of Neurology, Northwestern University Feinberg School of Medicine, Chicago, IL 60611, USA, [2]Department of Neuroscience, Mayo Clinic, Jacksonville, FL 32224, USA and [3]Department of Neurology, Mayo Clinic, Jacksonville, FL 32224, USA

*To whom correspondence should be addressed at: The Ken & Ruth Davee Department of Neurology, Northwestern University Feinberg School of Medicine, 303 E. Chicago Ave, Ward 12-140, Chicago, IL 60611, USA. Tel: +1 3125033936; Fax: +1 3125033951; Email: dkrainc@nm.org

Abstract

Frontotemporal dementia (FTD) encompasses a group of neurodegenerative disorders characterized by cognitive and behavioral impairments. Heterozygous mutations in progranulin (*PGRN*) cause familial FTD and result in decreased PGRN expression, while homozygous mutations result in complete loss of PGRN expression and lead to the neurodegenerative lysosomal storage disorder neuronal ceroid lipofuscinosis (NCL). However, how dose-dependent *PGRN* mutations contribute to these two different diseases is not well understood. Using iPSC-derived human cortical neurons from FTD patients harboring *PGRN* mutations, we demonstrate that *PGRN* mutant neurons exhibit decreased nuclear TDP-43 and increased insoluble TDP-43, as well as enlarged electron-dense vesicles, lipofuscin accumulation, fingerprint-like profiles and granular osmiophilic deposits, suggesting that both FTD and NCL-like pathology are present in *PGRN* patient neurons as compared to isogenic controls. *PGRN* mutant neurons also show impaired lysosomal proteolysis and decreased activity of the lysosomal enzyme cathepsin D. Furthermore, we find that PGRN interacts with cathepsin D, and that PGRN increases the activity of cathepsin D but not cathepsins B or L. Finally, we show that granulin E, a cleavage product of PGRN, is sufficient to increase cathepsin D activity. This functional relationship between PGRN and cathepsin D provides a possible explanation for overlapping NCL-like pathology observed in patients with mutations in *PGRN* or *CTSD*, the gene encoding cathepsin D. Together, our work identifies PGRN as an activator of lysosomal cathepsin D activity, and suggests that decreased cathepsin D activity due to loss of PGRN contributes to both FTD and NCL pathology in a dose-dependent manner.

Introduction

Frontotemporal dementia (FTD) is the second most common cause of dementia under the age of 65 (1,2). Up to half of all FTD patients have a family history of dementia, suggesting a strong genetic component of the disease (3–6). Importantly, pathogenic heterozygous mutations in the gene encoding progranulin (*PGRN*), which result in decreased (~50%) PGRN expression (7–10), account for 25% of familial FTD (9,11,12). PGRN is expressed in neurons and microglia (13) and has been implicated in inflammation (14–16), wound repair (17–19) and neurite outgrowth (20–22), but the mechanism by which FTD mutations in *PGRN* lead to neurodegeneration remain unclear.

Received: June 14, 2017. **Revised:** August 9, 2017. **Accepted:** August 24, 2017

Recently, several lines of evidence have suggested a potential role for PGRN in regulating lysosomal function. First, PGRN localizes to lysosomal compartments where it is subsequently cleaved into 7.5 individual granulins (23–25). Second, homozygous *PGRN* mutations lead to a complete loss of PGRN and cause neuronal ceroid lipofuscinosis (NCL) (26,27), a neurodegenerative lysosomal storage disorder. Finally, the neuropathology of aged *pgrn* knockout mice show indicators of an impaired autophagy-lysosome degradation system, including p62 inclusions (28) and accelerated lipofuscin accumulation (29). *pgrn* knockout mice also demonstrate increased immunoreactivity for the lysosomal membrane protein LAMP1 and increased expression of several lysosome-related genes (28). Together, these studies suggest that impaired lysosomal function may represent an important pathway leading to *PGRN*-linked neurodegeneration.

Here, we generated induced pluripotent stem cell (iPSC)-derived cortical neurons from an FTD patient with a heterozygous *PGRN* mutation to examine the role of PGRN in regulating lysosomal function. Surprisingly, we observed both FTD and NCL-like pathological hallmarks, as well as impaired lysosomal proteolysis and decreased activity of the lysosomal enzyme cathepsin D in FTD patient neurons. Homozygous mutations in the gene encoding cathepsin D (*CTSD*) lead to a form of NCL similar to those caused by homozygous mutations in *PGRN* (26,27,30–32). Furthermore, cathepsin D is predominantly expressed in the brain (33,34) where it is responsible for the degradation of long-lived proteins (35,36), but how its enzymatic activity is regulated within the lysosome is not well understood. Our results identify PGRN and its cleaved product, granulin E, as important activators of cathepsin D, but not cathepsins B and L, activity. We propose that dose-dependent loss of PGRN in both FTD and NCL result in decreased cathepsin D activity, contributing to defective lysosomal function in the pathogenesis of both neurodegenerative diseases.

Results

iPSC-derived cortical neurons from an FTD patient with a *PGRN* mutation exhibit both FTD and NCL-like pathological hallmarks

To investigate the role of PGRN in regulating lysosomal function in human neurons, we generated iPSC-derived cortical neurons from an FTD patient with a heterozygous *PGRN* mutation to examine how *PGRN* mutations may lead to neurodegeneration. We obtained patient-derived iPSCs harboring an FTD-linked heterozygous *PGRN* mutation (c.26 C > A, p.A9D) (10) (Supplementary Material, Fig. S1A). To properly characterize disease phenotypes, we also used previously established CRISPR/Cas9 genome editing protocols (37) to correct the *PGRN* mutation and generate an isogenic control line (*PGRN* WT). Correction of the *PGRN* mutation in the iPSC line was confirmed by Sanger sequencing (Supplementary Material, Fig. S1B) and resulted in increased PGRN expression in both *PGRN* WT iPSCs (Supplementary Material, Fig. S1C) and iPSC-derived neurons (Fig. 1A). Additionally, previous studies demonstrated that FTD patients with a *PGRN* mutation who carry an additional single nucleotide polymorphism (SNP) in the lysosomal membrane protein *TMEM106B* (transmembrane protein 106B) present with an earlier onset and increased severity of FTD (38). *PGRN* WT and mutant iPSC lines used in this study are heterozygous for the most common *TMEM106B* SNPs (rs1990622, rs6966915 and rs1020004) (Supplementary Material, Fig. S1D), a genotype not associated with increased risk and severity of FTD. Furthermore, g-band karyotype analysis demonstrated no chromosomal abnormalities (Supplementary Material, Fig. S2A and B) and additional characterization demonstrated that both *PGRN* WT and mutant iPSC lines expressed the pluripotency markers Nanog, Oct-4, SSEA-4 and Tra-1–81 (Supplementary Material, Fig. S3A).

We then differentiated both patient-derived *PGRN* WT and mutant iPSCs into human cortical neurons, the cell type predominantly affected in FTD. Using a previously described protocol (39), we successfully generated pure populations of glutamatergic neurons (≥98% MAP2 and vGLUT1/2 positive) (Supplementary Material, Fig. S3B) that expressed the cortical neuron markers Brn2 and Cux1 in both *PGRN* WT and mutant lines (Supplementary Material, Fig. S3C and D).

Utilizing iPSC-derived human cortical neurons from an FTD patient, we found that *PGRN* mutant neurons exhibited typical pathogenic hallmarks of FTD. At day 35 post-differentiation, *PGRN* mutant neurons showed decreased nuclear TDP-43 (TAR DNA-binding protein 43) as compared to *PGRN* WT neurons (Fig. 1B), consistent with what was previously observed in FTD patient brains (40–42). Moreover, we observed a time-dependent effect on insoluble TDP-43 accumulation, where the levels of insoluble TDP-43 were not significantly altered day 35 post-differentiation (Fig. 1C and D) but significantly increased in *PGRN* mutant neurons by day 100 post-differentiation as compared to *PGRN* WT neurons (Fig. 1C and D). These observations were consistent with previous studies which suggest that TDP-43 cytoplasmic mislocalization from the nucleus precedes its aggregation (41,43–45).

While heterozygous *PGRN* mutations lead to FTD (7–9,12), homozygous *PGRN* mutations result in the lysosomal storage disorder NCL (26,27). We next examined if *PGRN* mutant neurons from FTD patients could also develop pathological NCL phenotypes. Surprisingly, we found that *PGRN* mutant neurons also showed several hallmarks of NCL-like pathology. Using electron microscopy analysis, we observed accumulation of enlarged electron-dense vesicles in *PGRN* mutant neurons as compared to *PGRN* WT neurons (day 130 post-differentiation) (Fig. 1E and F). Additionally, we examined if *PGRN* mutant neurons from FTD patients also showed accumulation of lipofuscin, an autofluorescent electron-dense aggregate of undigested lysosomal material characteristically found in NCL patients (46). Using immunofluorescence to examine the levels of autofluorescent puncta in *PGRN* WT and mutant neurons (Fig. 1G), we found that *PGRN* mutant neurons showed a significant increase in lipofuscin puncta as compared to *PGRN* WT neurons (Fig. 1H). Finally, *PGRN* mutant neurons also showed electron-dense vesicles containing fingerprint-like profile patterns (Fig. 1I) and frequently contained granular osmiophilic deposits (Fig. 1J), two important characteristics of NCL pathology.

Together, these data demonstrate that iPSC-derived *PGRN* mutant cortical neurons from FTD patients exhibit both FTD and NCL-like phenotypes, and suggest that neurodegeneration due to *PGRN* mutations in FTD and NCL may share an underlying cellular mechanism.

iPSC-derived *PGRN* mutant neurons have impaired lysosomal function and reduced cathepsin D activity

Since *PGRN* mutant neurons from FTD patients develop features of the lysosomal storage disorder NCL, we examined if FTD-linked *PGRN* mutations lead to impaired lysosomal function. We measured lysosomal proteolysis in iPSC-derived FTD-linked

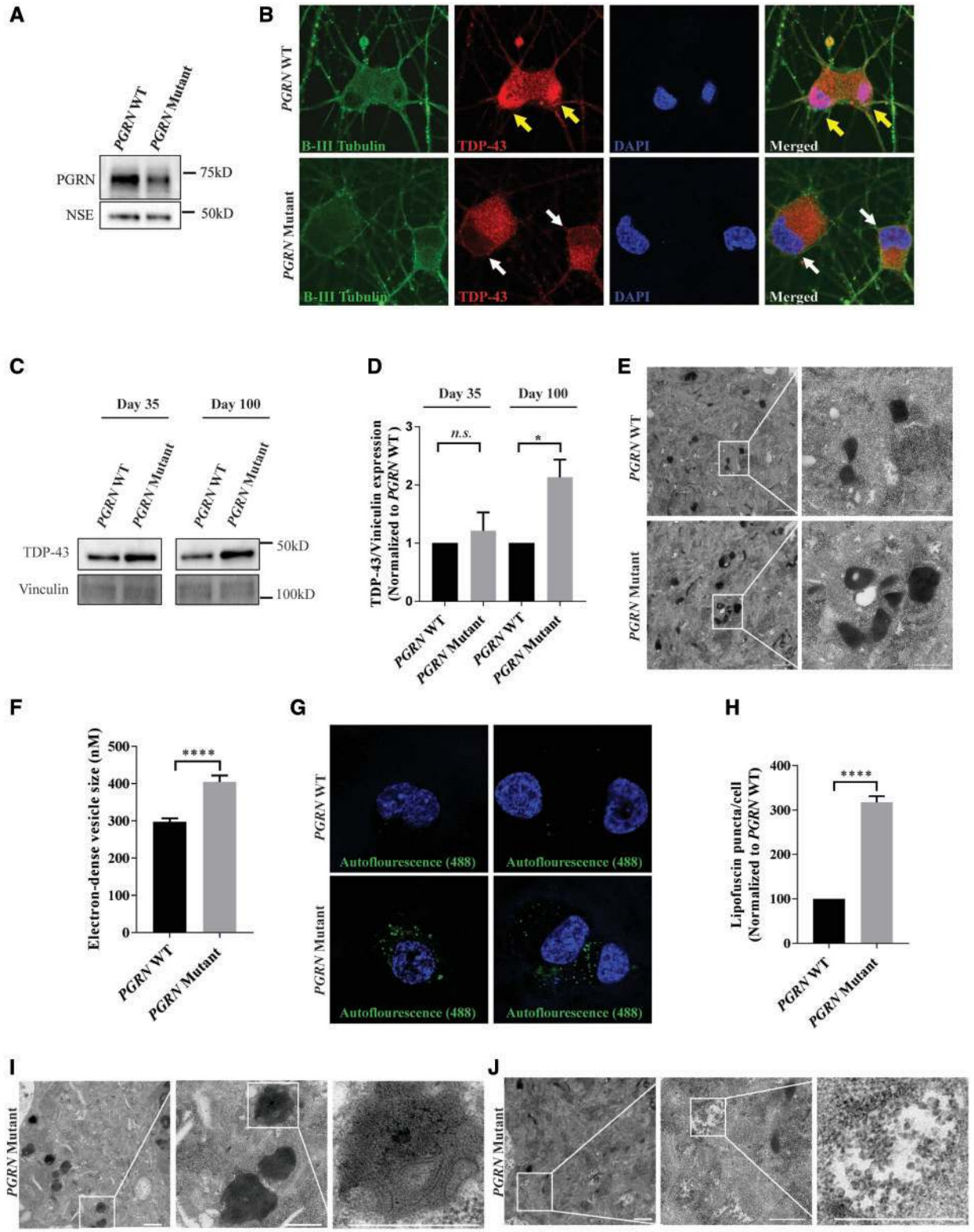

Figure 1. FTD-linked *PGRN* mutant neurons exhibit both FTD and NCL-like pathology. (**A**) PGRN expression in *PGRN* WT and mutant iPSC-derived neurons (day 35 post-differentiation) using NSE, a neuronal marker, as a loading control. (**B**) Immunofluorescence of TDP-43 and neuronal marker β-III tubulin in *PGRN* WT and mutant neuronal cultures (day 35 post-differentiation). *PGRN* mutant neurons have decreased nuclear TDP-43 (white arrows) as compared to *PGRN* WT neurons (yellow arrows). (**C**) Insoluble TDP-43 in *PGRN* WT and mutant neuron lysates (days 35 and 100 post-differentiation) shown by Western blot analysis using vinculin as a loading control. (**D**) Quantification of insoluble TDP-43 in *PGRN* WT and mutant neuron lysates (days 35 and 100 post-differentiation) ($n = 3$). (**E**) Electron dense vesicles in *PGRN* WT and mutant neurons (day 130 post-differentiation) visualized through electron microscopy analysis. Scale bar, 500 nM. (**F**) Quantification of electron-dense vesicle size in *PGRN* WT and mutant neurons (day 130 post-differentiation) ($n = 6$–8 cells/line). (**G**) Autofluorescent puncta in *PGRN* WT and mutant neurons (day 130 post-differentiation). (**H**) Quantification of lipofuscin puncta/cell in *PGRN* WT and mutant neurons (day 130 post-differentiation) ($n = 3$, 30–50 cells/experiment). Electron microscopy analysis of *PGRN* mutant neurons (day 130 post-differentiation) showed (**I**) fingerprint-like profiles and (**J**) granular osmiophilic deposits ($n = 6$–8 cells/line). Scale bar, 500 nM. Student's *t*-test, unpaired, two-tailed statistical analysis was performed. Error bars represent S.E.M. of total experiments. n.s., not significant, $^{*}P < 0.05$, $^{****}P < 0.0001$.

PGRN WT and mutant cortical neurons using a previously described radioactive pulse-chase analysis (47) and found that lysosomal proteolysis was significantly decreased in *PGRN* mutant neurons as compared to *PGRN* WT neurons (day 35 post-differentiation) (Fig. 2A). Additionally, Western blot (Fig. 2B–D) and immunofluorescence (Fig. 2E and F) analysis demonstrate that this decrease in lysosomal proteolysis was not due to a decrease in lysosomal density.

To investigate the mechanism by which *PGRN* mutations impair lysosomal function, we next examined if *PGRN* mutations altered the expression or activity of the lysosomal enzyme cathepsin D in iPSC-derived *PGRN* WT and mutant cortical neurons. Cathepsin D is widely expressed in the brain (33,34) and is the principle aspartyl protease responsible for degradation of long-lived proteins (35,36). Additionally, deficiencies in both PGRN and cathepsin D produce similar NCL phenotypes (30,31,46). In our heterozygous *PGRN* mutant iPSC-derived cortical neurons, we found that cathepsin D activity was significantly decreased in a time-dependent manner (at day 100, but not day 35 post-differentiation), as compared to *PGRN* WT neurons (Fig. 3A).

Western blot analysis demonstrated that this decrease in cathepsin D activity was not due to decreased expression of mature cathepsin D (Fig. 3B). In contrast, we observed an increase in mature cathepsin D at day 35 post-differentiation (Fig. 3D), as well as altered processing of cathepsin D (mature/immature levels) in *PGRN* mutant neurons as compared to WT neurons (Fig. 3E and F). We further showed that cathepsin D enzyme activity normalized to levels of mature cathepsin D was significantly decreased at both day 35 and day 100 post-differentiation in *PGRN* mutant neurons (Fig. 3G). Importantly, we did not see any changes in mature or immature levels of cathepsin B (Fig. 3C, Supplementary Material, Fig. S4A and B) or altered processing of cathepsin B (Supplementary Material, Fig. S4C) in *PGRN* mutant neurons.

To further investigate the relationship between PGRN and cathepsin D, we expressed both PGRN and cathepsin D in HEK293 cells and found that PGRN co-immunoprecipitated with cathepsin D (Fig. 3H), demonstrating that PGRN and cathepsin D interact with one another. In contrast, we did not see any interaction between PGRN and cathepsin B (Supplementary Material, Fig. S4D).

PGRN and granulin E are activators of cathepsin D activity

To determine if PGRN directly regulates cathepsin D activity, we performed *in vitro* cathepsin D activity assays using recombinant cathepsin D and PGRN. We found that recombinant PGRN was able to increase the activity of cathepsin D in a dose-dependent manner (Fig. 4A). However, PGRN did not increase the activities of either cathepsin B or L (Fig. 4B and C).

Since PGRN is cleaved into 7.5 individual granulins within the lysosome (48), we also compared the efficiencies of full-length PGRN versus cleaved granulins on activating cathepsin D. Granulins were obtained by proteolytic cleavage of recombinant PGRN with elastase (19) (Fig. 4D and E). At low concentrations (0.12 nM), cleaved granulins but not full-length PGRN, were able to significantly increase the activity of cathepsin D (Fig. 4F). These data suggest that while PGRN can increase cathepsin D activity, cleaved granulins are a more potent activator.

Finally, to examine which of the individual cleaved granulins may regulate cathepsin D activity, we performed *in vitro* cathepsin D activity assays using recombinant granulin E and granulin C. The purity of recombinant granulins E and C were confirmed by silver stain (Supplementary Material, Fig. S5A). Surprisingly, we found that while granulin C did not affect cathepsin D activity, granulin E was able to significantly increase the activity of cathepsin D in a dose-dependent manner (Fig. 4G). Importantly, using an antibody specific for granulin E (Supplementary Material, Fig. S5B), we were able to detect both full-length PGRN and granulin E in lysosome-enriched fractions (Fig. 4H).

Discussion

Using iPSC-derived cortical neurons from a heterozygous *PGRN* patient with FTD, we demonstrated that decreased PGRN expression in these neurons led to decreased cathepsin D activity and defective lysosomal function. We further found that PGRN interacts with cathepsin D, and that both full-length PGRN and one of its cleavage products, granulin E, were able to increase cathepsin D activity *in vitro* in a dose-dependent manner. Importantly, PGRN did not interact with cathepsin B, or increase the activities of cathepsins B and L. Taken together, our results provide important insight into both the normal role of PGRN in regulating cathepsin D activity and the cellular mechanisms by which *PGRN* mutations may cause FTD.

We were also able to recapitulate time-dependent progression of both FTD and NCL-like phenotypes in FTD neurons. FTD patients with *PGRN* mutations present with ubiquitin-positive inclusions in which TDP-43 is the main component (12,49–51). Previous reports on FTD patient pathology demonstrated that the loss of nuclear TDP-43 precedes the formation of TDP-43 insoluble aggregates (41,43–45), similar to what we observed in patient-derived neurons. Additionally, we found that FTD-linked *PGRN* mutant neurons developed phenotypes similar to characteristic hallmarks of NCL patient pathology including lipofuscin accumulation and the appearance of fingerprint-like profiles and granular osmiophilic deposits. These findings thus demonstrate the convergence of both FTD and NCL-like phenotypes in heterozygous *PGRN* mutant neurons from FTD patients, and further show the ability of iPSC patient-derived neurons to recapitulate time-dependent phenotypes in neurodegeneration, which are critical for providing insight into disease progression.

Previous studies have implicated a potential role for PGRN in lysosomal function, including its localization to lysosomes (23–25) and the accumulation of p62 (28) and lipofuscin (29) in *pgrn* knockout mice. Additionally, FTD patients with a *PGRN* mutation who carry SNPs in the lysosomal membrane protein *TMEM106B* present with an earlier onset and increased severity of FTD (38). While our *PGRN* mutant neurons carry the protective *TMEM106B* allele, we still observed dysfunctional lysosomes which resulted in increased lysosomal size, accumulation of lipofuscin and impaired lysosomal proteolysis. We propose that these changes are reflective of decreased cathepsin D activity due to decreased PGRN levels, rather than changes in the levels of lysosomal membrane proteins, which we did not observe. Interestingly, the granular osmiophilic deposits we observed in FTD-linked *PGRN* mutant neurons closely resembled those observed in the pathology of NCL patients with *CTSD* mutations, which lack cathepsin D activity (30,31), further suggesting that loss of cathepsin D function plays a key role in FTD-linked *PGRN* mutant pathogenesis. This link between PGRN and cathepsin D was also recently observed in several other models including human cell lines (52), *pgrn* knockout mice (53,54), and FTD patient fibroblasts and brain samples (55), further validating our observations in FTD patient iPSC-derived cortical neurons.

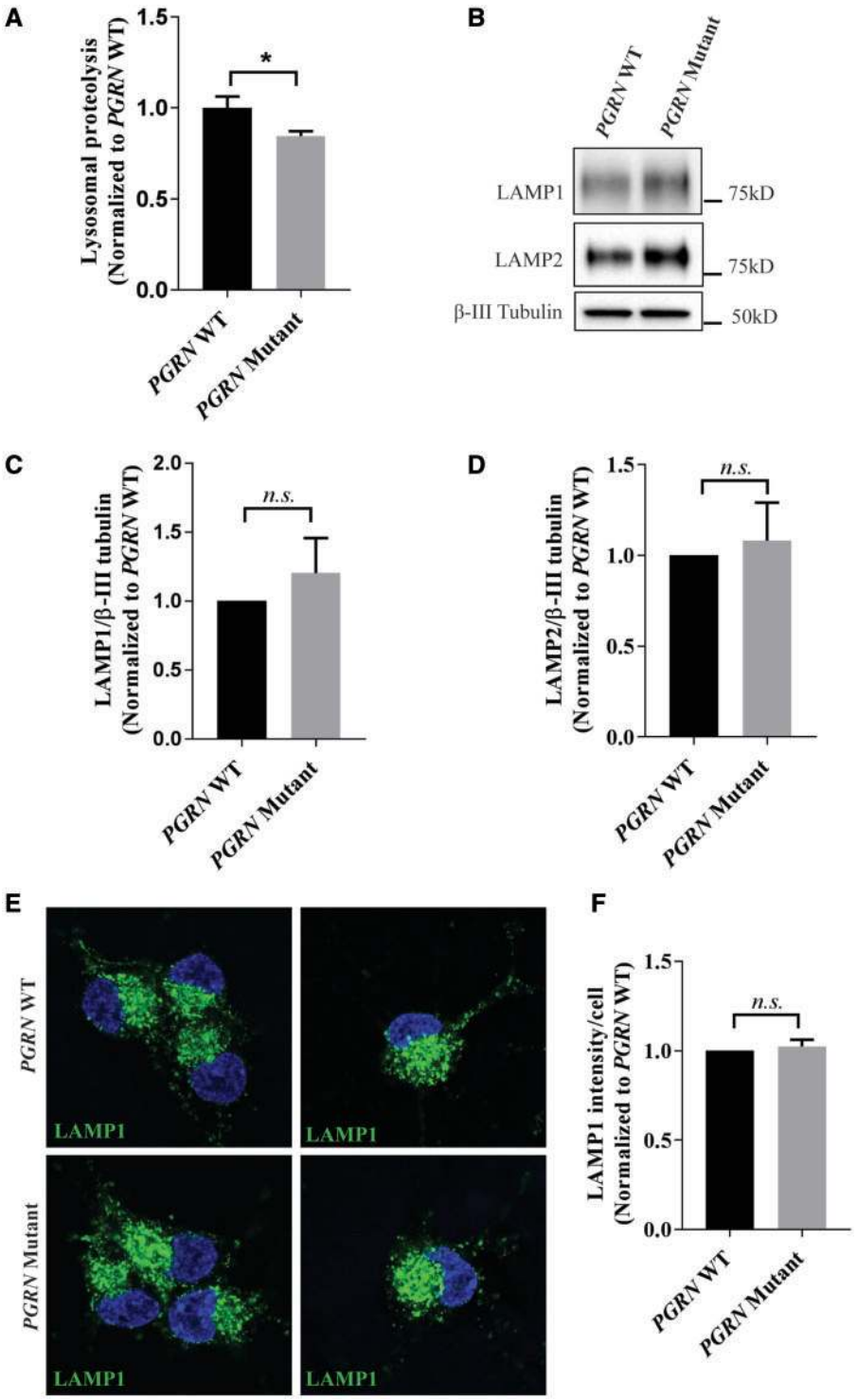

Figure 2. iPSC-derived *PGRN* mutant neurons have impaired lysosomal function. (**A**) Lysosomal proteolysis measured in *PGRN* WT and mutant cortical neurons (day 35 post-differentiation) through pulse-chase analysis ($n = 6$). (**B**) LAMP1 and LAMP2 expression in *PGRN* WT and mutant neuron lysates (day 35 post-differentiation) shown by Western blot analysis using β-III tubulin, a neuronal marker, as a loading control. Quantification of (**C**) LAMP1 and (**D**) LAMP2 expression in *PGRN* WT and mutant neuron lysates (day 35 post-differentiation) ($n = 3$). (**E**) Immunofluorescence of LAMP1 in *PGRN* WT and mutant neurons (day 35 post-differentiation). (**F**) Quantification of LAMP1 immunofluorescence intensity in *PGRN* WT and mutant neurons (day 35 post-differentiation) ($n = 3$, 95–114 cells/experiment). Student's *t*-test, unpaired, two-tailed statistical analysis was performed. Error bars represent S.E.M. of total experiments, n.s., not significant, $^*P < 0.05$.

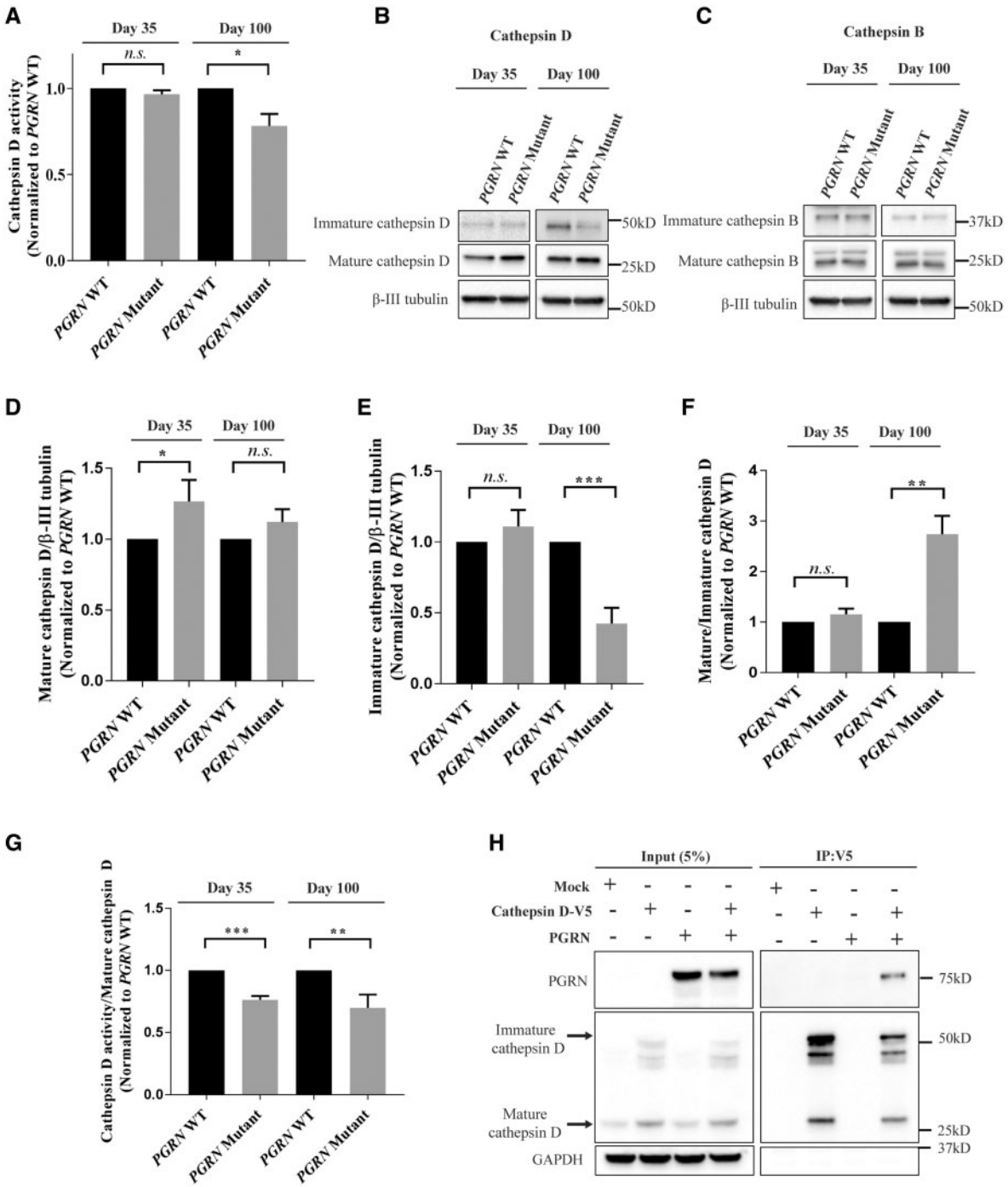

Figure 3. iPSC-derived *PGRN* mutant neurons have reduced cathepsin D activity. (**A**) Cathepsin D activity in *PGRN* WT and mutant cortical neuron lysates (days 35 and 100 post-differentiation) ($n = 3$). Immature and mature (**B**) cathepsin D and (**C**) cathepsin B expression in *PGRN* WT and mutant neuron lysates (days 35 and 100 post-differentiation) shown by Western blot analysis using β-III tubulin, a neuronal marker, as a loading control. Quantification of (**D**) mature and (**E**) immature cathepsin D expression in *PGRN* WT and mutant neuron lysates (days 35 and 100 post-differentiation) ($n = 3$). (**F**) Ratio of mature: immature cathepsin D in *PGRN* WT and mutant neuron lysates (days 35 and 100 post-differentiation) ($n = 3$). (**G**) Cathepsin D activity per mature cathepsin D expression in *PGRN* WT and mutant neuron lysates (35 and 100 days post-differentiation) ($n = 3$). (**H**) Co-immunoprecipitation assay in HEK293 cells co-expressing cathepsin D-V5 and PGRN show cathepsin D and PGRN interaction ($n = 3$). Student's *t*-test, unpaired, two-tailed statistical analysis was performed. Error bars represent S.E.M. of total experiments, n.s., not significant, $^{*}P < 0.05$, $^{**}P < 0.01$, $^{***}P < 0.001$.

While previous activators of cathepsin D have not been identified, we now show that PGRN can modulate cathepsin D activity in both recombinant protein assays and patient-derived neurons. Importantly, homozygous *PGRN* and *CTSD* mutations lead to similar forms of NCL (30,31,46). PGRN is a precursor protein that is cleaved into 7.5 individual granulins within lysosomes (48). This is similar to prosaposin, a multifunctional protein that is cleaved into 4 individual saposins (saposins A-D)

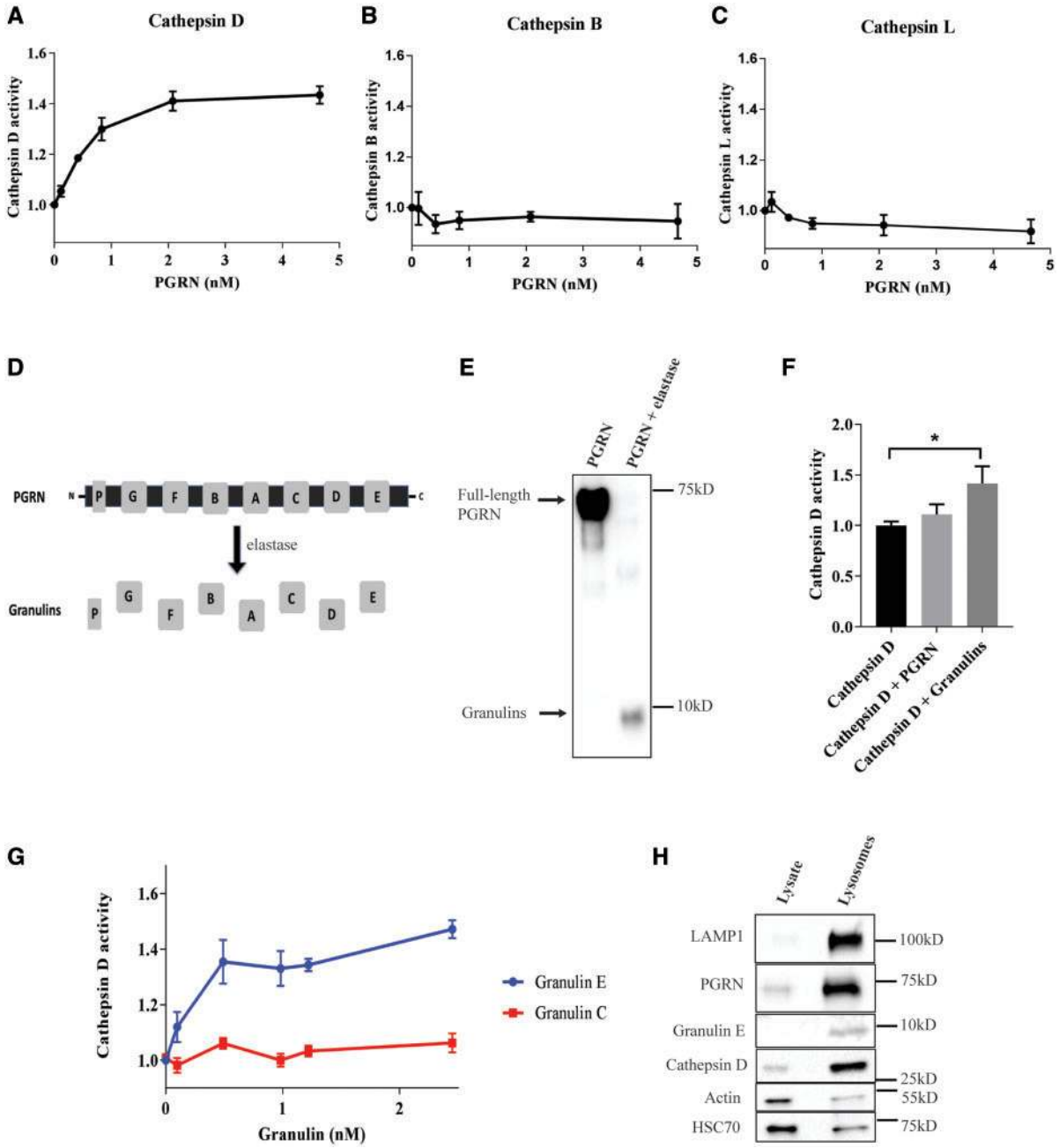

Figure 4. PGRN and granulin E are activators of cathepsin D activity. An *in vitro* dose-dependent (**A**) cathepsin D, (**B**) cathepsin B and (**C**) cathepsin L activity assay using recombinant cathepsins and recombinant PGRN ($n = 3$). (**D**) Structure of the human PGRN protein. PGRN is a precursor protein that can be enzymatically cleaved into 7.5 individual granulin motifs by the protease elastase. (**E**) Western blot analysis demonstrates effective cleavage of recombinant PGRN (0.12 nM) after incubation with elastase to obtain granulin sample. (**F**) Cathepsin D activity assay using recombinant cathepsin D incubated with either recombinant PGRN or granulins ($n = 3$). (**G**) A dose-dependent cathepsin D activity assay using recombinant cathepsin D incubated with either recombinant granulin E or granulin C ($n = 3$). (**H**) Western blot analysis of total cell lysate and lysosome-enriched samples in HEK293 cells ($n = 3$). Student's *t*-test, unpaired, two-tailed statistical analysis was performed. Error bars represent S.E.M of total experiments, n.s., not significant, $^*P < 0.05$.

within lysosomes (56). Individual saposins are able to act as lysosomal activators by promoting sphingolipid hydrolysis through activation of different lysosomal enzymes (57–61). Furthermore, loss or dysfunction of individual saposins results in distinct lysosomal storage disorders (62–65). Our work suggests that PGRN may be similar to prosaposin in its ability to be cleaved into individual granulins which subsequently activate specific lysosomal enzymes. We found that granulin E, but not granulin C was able to increase cathepsin D activity, suggesting specificity of the individual granulins on activating lysosomal enzymes.

Cathepsin D is an aspartyl protease, whereas cathepsins B and L are cysteine proteases. While we found that PGRN could both bind and activate cathepsin D activity, PGRN did not increase the activities of cathepsins B and L. Furthermore, we showed that PGRN did not interact with cathepsin B, suggesting that PGRN may have a preferential effect on cathepsin D rather than play a general role in the activation of cathepsins. Of note,

as we only showed preferential effect of full-length PGRN on cathepsin D in our study, it is still possible that individual granulins may have a role in the activation of additional cathepsin other than cathepsin D. In addition, as we found that the processing of cathepsin D, but not cathepsin B, was altered in *PGRN* mutant neurons, further studies will be required to examine how PGRN affects cathepsin D stability and maturation.

Heterozygous *PGRN* mutations lead to FTD while homozygous *PGRN* mutations lead to NCL. Although the convergence of these two diseases was previously unclear, our work demonstrates that FTD-linked heterozygous *PGRN* mutations are also able to cause NCL-like phenotypes in patient-derived FTD neurons. We propose that the neurodegeneration due to *PGRN* mutations in FTD and NCL may share an underlying cellular mechanism caused by decreased lysosomal cathepsin D activity, whereby partial loss of PGRN in FTD results in impaired lysosomal function, and complete loss of PGRN in NCL leads to severe lysosomal dysfunction.

Materials and Methods

Generation of induced pluripotent stem cells and neuronal differentiation

An FTD patient-derived fibroblast line with a heterozygous *PGRN* mutation (c.26 C > A, p.A9D) (10) was reprogramed by the Stem Cell Core Facility at Northwestern University (http://hms.facilities.northwestern.edu/; date last accessed Septemeber 28, 2017) to generate iPSCs. *PGRN* WT and mutant iPSC lines used in this study were heterozygous for the most common *TMEM106B* SNPs (rs1990622, rs6966915 and rs1020004). iPSC lines were shown to express the pluripotency markers Nanog, Oct4, SSEA-4 and Tra-1–81 through immunofluorescence analysis and g-band karyotype analysis was performed by Cell Line Genetics (https://www.clgenetics.com/; date last accessed Septemeber 28, 2017).

An isogenic control line (*PGRN* WT) was generated using a previously established CRISPR/Cas9 genome editing protocol (37). Guide RNAs were cloned into plasmid expressing Cas9 D10A nickase (px461) containing 2 A-GFP to allow for selection of cells and a single-stranded DNA oligonucleotide (ssODN) (generated by Integrated DNA Technologies) was designed as a repair template. CRISPR/Cas9 plasmid and ssODN delivery into iPSC cells was performed using Neon® Transfection System (ThermoFisher). 30 h after transfection, the cells were FACS sorted at the Northwestern University Flow Cytometry Core (https://rhlccflow.facilities.northwestern.edu/; date last accessed Septemeber 28, 2017) to select for transfected cells. After colonies reached a sufficient size, they were manually picked and expanded. Genomic DNA was isolated from each clone using Direct PCR Lysis Reagent (Cell) (Viagen Biotech, 301-C) and used for Sanger sequencing to identify clones with corrected mutations. Sanger sequencing was performed by the University of Chicago Comprehensive Cancer Center DNA Sequencing and Genotyping Facility (http://cancer-seqbase.uchicago.edu/; date last accessed Septemeber 28, 2017).

PGRN WT and mutant iPSCs were differentiated into cortical glutamatergic neurons using a previously described protocol (39). It was previously demonstrated that cortical neurons produced using this protocol form functional synapses at day 21 (39).

Electron microscopy analysis

Northwestern University's Center for Advanced Microcopy (https://cam.facilities.northwestern.edu/; date last accessed Septemeber 28, 2017) processed and sectioned *PGRN* WT and mutant neuron samples (day 130 post-differentiation) for transmission electron microscopy (TEM) analysis. Images were taken using FEI Tecnai Spirit G2 TEM.

Antibodies

The antibodies used in this study were: TDP-43 (Protein Tech, 12892–1-AP), Vinculin (Abcam, ab18058), LAMP1 (DSHB Hybridoma, H4A3-s) (for Western blots), LAMP1 (Santa Cruz, sc-20011) (for immunofluorescence), LAMP2 (DSHB Hybridoma, H4B4-s), Cathepsin D (Abcam, ab75852), cathepsin B (R&D, AF953) (for Western blots), cathepsin B (Abcam, ab125067) (for co-immunoprecipitation assay), GAPDH (Millipore, MAB374), B-III tubulin (Biolegend, 801201), MAP2 (Sigma, M4403), PGRN (Abcam, ab108608), GRN E (Anti-granulin C-terminal) (Sigma, SAB4200310), NSE (ThermoFisher, PA5–12374), VGLUT1/2 (Synaptic Systems, 135303), Brn2 (Cell Signaling, 12137) and CUX1 (Santa Cruz, sc-13024). All antibodies were used at a 1: 1000 dilution for Western blot analysis (in 5% Bovine Serum Albumin, 0.5% Sodium Azide) and a 1: 200 dilution for immunofluorescence analysis (in 5% normal goat serum, 1% BSA).

We confirmed that the anti-granulin C-terminal (Sigma, SAB4200310) antibody was specific for granulin E. Overexpression vectors of individual granulins (petite granulin and granulins A-G) (cloned into pcDNA3.1/His vector) were provided by the Van Damme laboratory (Leuven, Belgium). HEK293 cells were transfected with a total of 0.5 μg of plasmid DNA for each sample using Lipofectamine® (Invitrogen, 11668–019) and collected 48 h post-transfection in NP-40 lysis buffer (1% NP-40, 150 mM NaCl, 50 mM Tris-HCl, pH 5.0) containing cOmplete™, Mini, EDTA-free Protease Inhibitor Cocktail (Roche, 11836170001). The samples were lysed on ice for 30 min, centrifuged at 20 000 g for 20 min and then analysed through Western blot analysis.

Western blot analysis

Western blot analysis was performed using cellular lysates from *PGRN* WT and mutant cortical neurons. *PGRN* mutant and control neuron samples were collected at specific time points (days 35 and 100 post-differentiation) in Triton-X Buffer (1% Triton X-100, 20 mM HEPES, 150 mM NaCl, 10% Glycerol, 1 mM EDTA, 1.5 mM $MgCl_2$) containing cOmplete™, Mini, EDTA-free Protease Inhibitor Cocktail (Roche, 11836170001). The samples were homogenized on ice and subsequently centrifuged at 100 000 g for 30 min to obtain the triton soluble fraction. The Triton-insoluble pellet was resuspended in SDS buffer (2% SDS, 50 mM Tris pH 7.4), boiled, sonicated and then centrifuged at 20 000 g for 20 min to obtain Triton-insoluble fraction. Fractions were then analysed through Western blot analysis.

PGRN WT and mutant neuron samples used to detect levels of immature/mature cathepsin B and D were collected in NP-40 lysis buffer (1% NP-40, 150 mM NaCl, 50 mM Tris-HCl, pH 5.0) containing cOmplete™, Mini, EDTA-free Protease Inhibitor Cocktail (Roche, 11836170001). The samples were homogenized on ice and subsequently centrifuged at 20 000 g for 20 min. Samples were then analysed through Western blot analysis. The same western blot of neuron lysates was used to immunoblot both cathepsin D and cathepsin B.

Immunofluorescence

PGRN WT and mutant neurons were plated onto nitric-acid treated glass coverslips and fixed with 4% formaldehyde for

10 min. Neurons were then blocked and permeabilized using blocking buffer (5% normal goat serum, 1% BSA, 0.1% saposin) for 30 min at room temperature. Neurons were incubated at 4 °C with primary antibody overnight and secondary antibody for 2 h at room temperature in blocking buffer. The coverslips were mounted using VECTASHIELD Hard Set Antifade Mounting Medium with DAPI (Vector Laboratories, H-1500). Images were subsequently taken using a Leica confocal microscope at 63X magnification and analysed using Fiji software.

Samples for lipofuscin analysis were mounted after fixation (without incubation with primary or secondary antibodies). Images of autoflourescent signal were taken using the 488 channel.

Analysis of lysosomal proteolysis

Lysosomal proteolysis was measured in *PGRN* WT and mutant neurons samples (day 35 post-differentiation) using a previously described radioactive pulse-chase analysis (47). In this assay, ^{3}H-leucine (Perkin Elmer, NET460A001MC) was added to the media of neuron cultures and subsequently removed after 48 h. Media samples were then taken at multiple time points (8, 20 and 28 h) to determine the level of radioactivity in the media. The portion of soluble radioactivity in the media was used as a measure of total proteolysis. Additional neurons were treated with 20 mM NH_4Cl (Sigma, A4514) and 200 μM leupeptin (Millipore, 108976) in combination with ^{3}H-leucine as a measure of non-lysosomal proteolysis. Non-lysosomal proteolysis was subtracted from the total proteolysis to determine the level of lysosomal proteolysis.

Dose-dependent cathepsin D, cathepsin B and cathepsin L activity assays

In vitro dose-dependent fluorometric activity assays were performed using recombinant cathepsin D (Sigma, C3138), cathepsin B (BioVision, 7408–10), cathepsin L (R&D, 952-CY-010) and PGRN (R&D, 2420-PG-050). Recombinant granulins C and E were produced by VIB's protein service facility (PSF, Ghent, Belgium) and provided by the Van Damme laboratory (Leuven, Belgium). To confirm purity, 7 ng of recombinant granulins C and E were loaded and run on a 14% tris-glycine gel (ThermoFisher, XP00142BOX). A silver stain kit (ThermoFisher, 24612) was then used to detect proteins within the sample.

For cathepsin D activity assays, recombinant cathepsin D was diluted to 20 μg/ml in assay buffer (citrate buffer pH 3.6, 1% BSA, 0.05% Tween) and activated by incubation at 37 °C for 30 min. Cathepsin D fluorogenic substrate (Mca-Pro-Leu-Gly-Leu-Dpa-Ala-Arg-NH2) (Enzo, BML-P145–0001) was diluted to 40 μM in the assay buffer. The activity assay was performed in a black, flat bottom 96-well plate (ThermoFisher, 475515), where recombinant cathepsin D and cathepsin D fluorogenic substrate were added at a final concentration of 0.53 nM and 10 μM, respectively. Additionally, samples containing increasing levels of PGRN (final concentrations 0–4.7 nM) or granulins were prepared. Granulin samples were prepared by proteolytic cleavage of PGRN (0.12 nM) with elastase (Athens Research and Technology, 16–14-051200) for 30 min at 37 °C. A control sample containing cathepsin D and elastase demonstrated that elastase does not affect cathepsin D activity. A standard curve was also prepared for each plate. The 96-well plate was incubated at 37 °C for 25 min and cathepsin D activity was subsequently measured at an excitation wavelength of 328 nM and emission wavelength of 393 nM.

In addition, *in vitro* dose-dependent fluorometric cathepsin D activity assays were performed using recombinant granulin E and granulin C. These assays were performed as described above but used samples containing increasing levels of either recombinant granulin E or granulin C (final concentrations 0–2.45 nM).

For cathepsin B activity assays, recombinant cathepsin B was diluted to 10 μg/ml in activation buffer (25 mM MES, 5 mM DTT, pH 5.0) and activated by incubation for 15 min at room temperature. Cathepsin B substrate (OMNICATHEPSIN® fluorogenic substrate) (Enzo, BML-P139–0010) was diluted to 20 μM in assay buffer (25 mM MES, pH 5.0). The activity assay was performed in a black, flat bottom 96-well plate (ThermoFisher, 475515), where recombinant cathepsin B and cathepsin B fluorogenic substrate were added at a final concentration of 0.53 nM and 10 μM, respectively. Additionally, samples containing increasing levels of PGRN (final concentrations 0–4.7 nM) and a standard curve was prepared for each plate. The 96-well plate was incubated at 37 °C for 30 min and cathepsin B activity was subsequently measured at an excitation wavelength of 380 nM and emission wavelength of 460 nM.

For cathepsin L activity assays, recombinant cathepsin L was diluted to 40μg/ml in assay buffer [50 mM MES, 5 mM DTT, 1 mM EDTA, 0.005% (w/v) Brij-35, pH 6.0] and activated by incubation at 15 min on ice. Cathepsin L substrate (OMNICATHEPSIN® fluorogenic substrate) (Enzo, BML-P139–0010) was diluted to 20 μM in assay buffer. The activity assay was performed in a black, flat bottom 96-well plate (ThermoFisher, 475515), where recombinant cathepsin L and cathepsin L fluorogenic substrate were added at a final concentration of 0.48 nM and 1 μM, respectively. Additionally, samples containing increasing levels of PGRN (final concentrations 0–4.7 nM) and a standard curve was prepared for each plate. The 96-well plate was incubated at 37 °C for 2.5 min and cathepsin L activity was subsequently measured at excitation wavelength of 380 nM and emission wavelength of 460 nM.

SpectraMax i3 Multi-mode microplate reader was used for *in vitro* activity assays.

Cathepsin D activity assays in *PGRN* WT and mutant cortical neurons

Cathepsin D activity assays were performed using cellular lysates from *PGRN* WT and mutant cortical neurons. *PGRN* mutant and control neuron samples were collected at specific time points (days 35 and 100 post-differentiation) in enzyme activity lysis buffer (citrate buffer pH 3.6, 1% BSA, 0.1% Tween). Cells were homogenized on ice and subsequently centrifuged at 20 000 g for 20 min to remove cellular debris. The cathepsin D activity assay was performed in a black, flat bottom 96-well plate (ThermoFisher, 475515) using a cathepsin D fluorogenic substrate (final concentration of 10 μM) and 5 μg of cellular lysates in a final volume of 200 μl of assay buffer (citrate buffer pH 3.4, 1%BSA, 0.05% Tween). An additional set of each sample was prepared in the presence of the cathepsin D inhibitor pepstatin A (100 nM) (Enzo, ALX-260–085-M005) to determine cathepsin D activity. Cathepsin D activity was measured as previously described (see *Dose-dependent cathepsin D, cathepsin B and cathepsin L activity assays*).

Co-immunoprecipitation assay

PGRN and cathepsin D co-immunoprecipitation assay was performed in HEK293 cells. Overexpression vectors of cathepsin D

with an N-terminal V5 tag (cloned into pcDNA3.1/V5-His vector) and PGRN (cloned into pcDNA3.1 vector) were utilized for this assay. Each assay contained four sets of samples: empty vector (pcDNA3.1 vector) over-expression, cathepsin D-V5 over-expression, PGRN over-expression and cathepsin D-V5 + PGRN over-expression. HEK293 cells were transfected with a total of 2.5 μg of plasmid DNA for each sample using Lipofectamine® (Invitrogen, 11668–019) and collected 48 h post-transfection in CHAPS buffer (40 mM HEPES pH 7.4, 120 mM NaCl, 1 mM EDTA, 50 mM NaF, 0.3% CHAPS,) containing cOmplete™, Mini, EDTA-free Protease Inhibitor Cocktail (Roche, 11836170001). Cells were lysed on ice for 30 min and subsequently centrifuged at 20, 000 g for 20 min to remove cellular debris. Anti-V5 agarose beads (20 μl) (Sigma, A7345–1ML) were added to the cell lysis samples and rotated overnight at 4 °C. Samples were then centrifuged at 150 g for 3 min and washed 3 times with CHAPS buffer. Anti-V5 agarose beads were resuspended in 2X sample buffer after the final wash and samples were then analysed through Western blot analysis.

PGRN and cathepsin B co-immunoprecipitation assay was also performed in HEK293 cells. Overexpression vectors of cathepsin B (cloned into pcDNA3.1) (Addgene plasmid #11249) and PGRN (cloned into pcDNA3.1 vector) were utilized for this assay. Experiments used the same set of samples and transfection conditions as cathepsin D-PGRN co-immunoprecipitation assay (see previous paragraph). Cells were collected in EBC lysis buffer (Boston BioProducts, C-1410) containing cOmplete™, Mini, EDTA-free Protease Inhibitor Cocktail (Roche, 11836170001). Cells were lysed on ice for 30 min and subsequently centrifuged at 20 000 g for 20 min to remove cellular debris. 3μl of cathepsin B antibody was added to cell lysate for each sample and rotated at 4 °C for 30 min. Dynabeads (10 μl) were then added to cell lysate and rotated at room temperature for 10 min. The samples were then washed 3X for 5 min at room temperature with EBC lysis buffer. Dynabeads were resuspended in 2X sample buffer after the final wash. An IgG control (normal rabbit IgG) (Santa Cruz, sc-2027) was also performed for each sample. Samples were then analysed through Western blot analysis.

Lysosomal enrichment

Lysosome-enriched samples were generated from HEK293 cells using Lysosome Enrichment Kit for Tissues and Cultured Cells (ThermoFisher, 89839).

Statistical analysis

Student's *t*-test, unpaired, two-tailed statistical analysis was performed. *P*-values less than 0.05 were considered significant. Statistical analysis was performed using GraphPad Prism Software, Version 7.0 b.

Supplementary Material

Supplementary Material is available at *HMG* online.

Acknowledgements

We thank Dr. Taiji Tsunemi for his thoughtful advice and guidance. We are grateful to Maria Nguyen, Hyunkyung Jeong and Drs. Jessica McDonald and Niccolo Mencacci for valuable discussions and technical expertise. We thank Dr. Evangelos Kiskinis for his advise and technical expertise on cortical neuron differentiation and Dr. Anis Contractor for generously donating the constructs used for the differentiation. We thank Lennell Reynolds Jr. for EM assistance, and Paul Mehl for FACs assistance.

Conflict of Interest statement. None declared.

Funding

National Institutes of Health grants [R01 NS076054 and R37 NS096241 to D.K.], [5R25 GM079300–07 and 5T32 AG020506–13 to C.V], [T32 NS041234 and F32 NS101778 to Y.C.W.] and [P50 NS072187 to Z.W.], Human Embryonic and Induced Pluripotent Stem Cell Facility at Northwestern University (NIH core support grant P30 [NS081774]), Northwestern University Flow Cytometry Core (supported by NCI CCSG P30 [CA060553] awarded to the Robert H Lurie Comprehensive Cancer Center), Northwestern University Center for Advanced Microscopy (supported by NCI CCSG P30 [CA060553] awarded to the Robert H Lurie Comprehensive Cancer Center) and Mayo Clinic Center for Regenerative Medicine.

References

1. Onyike, C.U. and Diehl-Schmid, J. (2013) The epidemiology of frontotemporal dementia. *Int. Rev. Psychiatry*, **25**, 130–137.
2. Vieira, R.T., Caixeta, L., Machado, S., Silva, A.C., Nardi, A.E., Arias-Carrion, O. and Carta, M.G. (2013) Epidemiology of early-onset dementia: a review of the literature. *Clin. Pract. Epidemiol. Ment. Health*, **9**, 88–95.
3. Chow, T.W., Miller, B.L., Hayashi, V.N. and Geschwind, D.H. (1999) Inheritance of frontotemporal dementia. *Arch. Neurol.*, **56**, 817–822.
4. Rascovsky, K., Hodges, J.R., Knopman, D., Mendez, M.F., Kramer, J.H., Neuhaus, J., van Swieten, J.C., Seelaar, H., Dopper, E.G. and Onyike, C.U. (2011) Sensitivity of revised diagnostic criteria for the behavioural variant of frontotemporal dementia. *Brain*, **134**, 2456–2477.
5. Wood, E.M., Falcone, D., Suh, E., Irwin, D.J., Chen-Plotkin, A.S., Lee, E.B., Xie, S.X., Van Deerlin, V.M. and Grossman, M. (2013) Development and validation of pedigree classification criteria for frontotemporal lobar degeneration. *JAMA Neurol.*, **70**, 1411–1417.
6. Rohrer, J.D., Guerreiro, R., Vandrovcova, J., Uphill, J., Reiman, D., Beck, J., Isaacs, A.M., Authier, A., Ferrari, R., Fox, N.C. *et al.* (2009) The heritability and genetics of frontotemporal lobar degeneration. *Neurology*, **73**, 1451–1456.
7. Chiang, H.H., Rosvall, L., Brohede, J., Axelman, K., Bjork, B.F., Nennesmo, I., Robins, T. and Graff, C. (2008) Progranulin mutation causes frontotemporal dementia in the Swedish Karolinska family. *Alzheimers Dement.*, **4**, 414–420.
8. Mukherjee, O., Wang, J., Gitcho, M., Chakraverty, S., Taylor-Reinwald, L., Shears, S., Kauwe, J.S., Norton, J., Levitch, D., Bigio, E.H. *et al.* (2008) Molecular characterization of novel progranulin (GRN) mutations in frontotemporal dementia. *Hum. Mut.*, **29**, 512–521.
9. Baker, M., Mackenzie, I.R., Pickering-Brown, S.M., Gass, J., Rademakers, R., Lindholm, C., Snowden, J., Adamson, J., Sadovnick, A.D., Rollinson, S. *et al.* (2006) Mutations in progranulin cause tau-negative frontotemporal dementia linked to chromosome 17. *Nature*, **442**, 916–919.
10. Wider, C., Uitti, R.J., Wszolek, Z.K., Fang, J.Y., Josephs, K.A., Baker, M.C., Rademakers, R., Hutton, M.L. and Dickson, D.W. (2008) Progranulin gene mutation with an unusual clinical

and neuropathologic presentation. *Mov. Disord.*, **23**, 1168–1173.
11. Petkau, T.L. and Leavitt, B.R. (2014) Progranulin in neurodegenerative disease. *Trends Neurosci.*, **37**, 388–398.
12. Gass, J., Cannon, A., Mackenzie, I.R., Boeve, B., Baker, M., Adamson, J., Crook, R., Melquist, S., Kuntz, K., Petersen, R. *et al.* (2006) Mutations in progranulin are a major cause of ubiquitin-positive frontotemporal lobar degeneration. *Hum. Mol. Genet.*, **15**, 2988–3001.
13. Petkau, T.L., Neal, S.J., Orban, P.C., MacDonald, J.L., Hill, A.M., Lu, G., Feldman, H.H., Mackenzie, I.R. and Leavitt, B.R. (2010) Progranulin expression in the developing and adult murine brain. *J. Comp. Neurol.*, **518**, 3931–3947.
14. Yin, F., Banerjee, R., Thomas, B., Zhou, P., Qian, L., Jia, T., Ma, X., Ma, Y., Iadecola, C., Beal, M.F. *et al.* (2010) Exaggerated inflammation, impaired host defense, and neuropathology in progranulin-deficient mice. *J. Exp. Med.*, **207**, 117–128.
15. Tang, W., Lu, Y., Tian, Q.Y., Zhang, Y., Guo, F.J., Liu, G.Y., Syed, N.M., Lai, Y., Lin, E.A., Kong, L. *et al.* (2011) The growth factor progranulin binds to TNF receptors and is therapeutic against inflammatory arthritis in mice. *Science*, **332**, 478–484.
16. Mundra, J.J., Jian, J., Bhagat, P. and Liu, C.J. (2016) Progranulin inhibits expression and release of chemokines CXCL9 and CXCL10 in a TNFR1 dependent manner. *Sci. Rep.*, **6**, 21115.
17. He, Z., Ong, C.H., Halper, J. and Bateman, A. (2003) Progranulin is a mediator of the wound response. *Nat. Med.*, **9**, 225–229.
18. He, Z., Ismail, A., Kriazhev, L., Sadvakassova, G. and Bateman, A. (2002) Progranulin (PC-cell-derived growth factor/acrogranin) regulates invasion and cell survival. *Cancer Res.*, **62**, 5590–5596.
19. Zhu, J., Nathan, C., Jin, W., Sim, D., Ashcroft, G.S., Wahl, S.M., Lacomis, L., Erdjument-Bromage, H., Tempst, P., Wright, C.D. *et al.* (2002) Conversion of proepithelin to epithelins: roles of SLPI and elastase in host defense and wound repair. *Cell*, **111**, 867–878.
20. Van Damme, P., Van Hoecke, A., Lambrechts, D., Vanacker, P., Bogaert, E., van Swieten, J., Carmeliet, P., Van Den Bosch, L. and Robberecht, W. (2008) Progranulin functions as a neurotrophic factor to regulate neurite outgrowth and enhance neuronal survival. *J. Cell Biol.*, **181**, 37–41.
21. Gao, X., Joselin, A.P., Wang, L., Kar, A., Ray, P., Bateman, A., Goate, A.M. and Wu, J.Y. (2010) Progranulin promotes neurite outgrowth and neuronal differentiation by regulating GSK-3beta. *Protein Cell*, **1**, 552–562.
22. Petkau, T.L., Neal, S.J., Milnerwood, A., Mew, A., Hill, A.M., Orban, P., Gregg, J., Lu, G., Feldman, H.H., Mackenzie, I.R. *et al.* (2012) Synaptic dysfunction in progranulin-deficient mice. *Neurobiol. Dis.*, **45**, 711–722.
23. Almeida, S., Zhou, L., Gao, F.-B. and Iijima, K.M. (2011) Progranulin, a glycoprotein deficient in frontotemporal dementia, is a novel substrate of several protein disulfide isomerase family proteins. *PloS One*, **6**, e26454.
24. Hu, F., Padukkavidana, T., Vægter, C.B., Brady, O.A., Zheng, Y., Mackenzie, I.R., Feldman, H.H., Nykjaer, A. and Strittmatter, S.M. (2010) Sortilin-mediated endocytosis determines levels of the frontotemporal dementia protein, progranulin. *Neuron*, **68**, 654–667.
25. Tanaka, Y., Matsuwaki, T., Yamanouchi, K. and Nishihara, M. (2013) Increased lysosomal biogenesis in activated microglia and exacerbated neuronal damage after traumatic brain injury in progranulin-deficient mice. *Neuroscience*, **250**, 8–19.
26. Smith, K.R., Damiano, J., Franceschetti, S., Carpenter, S., Canafoglia, L., Morbin, M., Rossi, G., Pareyson, D., Mole, S.E., Staropoli, J.F. *et al.* (2012) Strikingly different clinicopathological phenotypes determined by progranulin-mutation dosage. *Am. J. Hum. Genet.*, **90**, 1102–1107.
27. Almeida, M.R., Macario, M.C., Ramos, L., Baldeiras, I., Ribeiro, M.H. and Santana, I. (2016) Portuguese family with the co-occurrence of frontotemporal lobar degeneration and neuronal ceroid lipofuscinosis phenotypes due to progranulin gene mutation. *Neurobiol. Aging*, **41**, 200 e201–205.
28. Tanaka, Y., Chambers, J.K., Matsuwaki, T., Yamanouchi, K. and Nishihara, M. (2014) Possible involvement of lysosomal dysfunction in pathological changes of the brain in aged progranulin-deficient mice. *Acta Neuropathol. Commun.*, **2**, 78.
29. Wils, H., Kleinberger, G., Pereson, S., Janssens, J., Capell, A., Van Dam, D., Cuijt, I., Joris, G., De Deyn, P.P. and Haass, C. (2012) Cellular ageing, increased mortality and FTLD-TDP-associated neuropathology in progranulin knockout mice. *J. Pathol.*, **228**, 67–76.
30. Siintola, E., Partanen, S., Stromme, P., Haapanen, A., Haltia, M., Maehlen, J., Lehesjoki, A.E. and Tyynela, J. (2006) Cathepsin D deficiency underlies congenital human neuronal ceroid-lipofuscinosis. *Brain*, **129**, 1438–1445.
31. Steinfeld, R., Reinhardt, K., Schreiber, K., Hillebrand, M., Kraetzner, R., Bruck, W., Saftig, P. and Gartner, J. (2006) Cathepsin D deficiency is associated with a human neurodegenerative disorder. *Am. J. Hum. Genet.*, **78**, 988–998.
32. Tyynela, J., Sohar, I., Sleat, D.E., Gin, R.M., Donnelly, R.J., Baumann, M., Haltia, M. and Lobel, P. (2000) A mutation in the ovine cathepsin D gene causes a congenital lysosomal storage disease with profound neurodegeneration. *EMBO J.*, **19**, 2786–2792.
33. Whitaker, J.N., Terry, L.C. and Whetsell, W.O. Jr. (1981) Immunocytochemical localization of cathepsin D in rat neural tissue. *Brain Res.*, **216**, 109–124.
34. Banay-Schwartz, M., DeGuzman, T., Kenessey, A., Palkovits, M. and Lajtha, A. (1992) The distribution of cathepsin D activity in adult and aging human brain regions. *J. Neurochem.*, **58**, 2207–2211.
35. Dean, R.T. (1979) Lysosomes and protein degradation. *Ciba Found. Symp.*, 139–149.
36. Hossain, S., Alim, A., Takeda, K., Kaji, H., Shinoda, T. and Ueda, K. (2001) Limited proteolysis of NACP/alpha-synuclein. *J. Alzheimers Dis.*, **3**, 577–584.
37. Ran, F.A., Hsu, P.D., Wright, J., Agarwala, V., Scott, D.A. and Zhang, F. (2013) Genome engineering using the CRISPR-Cas9 system. *Nat. Protoc.*, **8**, 2281–2308.
38. Van Deerlin, V.M., Sleiman, P.M., Martinez-Lage, M., Chen-Plotkin, A., Wang, L.S., Graff-Radford, N.R., Dickson, D.W., Rademakers, R., Boeve, B.F., Grossman, M. *et al.* (2010) Common variants at 7p21 are associated with frontotemporal lobar degeneration with TDP-43 inclusions. *Nat. Genet.*, **42**, 234–239.
39. Zhang, Y., Pak, C., Han, Y., Ahlenius, H., Zhang, Z., Chanda, S., Marro, S., Patzke, C., Acuna, C., Covy, J. *et al.* (2013) Rapid single-step induction of functional neurons from human pluripotent stem cells. *Neuron*, **78**, 785–798.
40. Arai, T., Hasegawa, M., Akiyama, H., Ikeda, K., Nonaka, T., Mori, H., Mann, D., Tsuchiya, K., Yoshida, M., Hashizume, Y. *et al.* (2006) TDP-43 is a component of ubiquitin-positive tau-negative inclusions in frontotemporal lobar degeneration and amyotrophic lateral sclerosis. *Biochem. Biophys. Res. Commun.*, **351**, 602–611.
41. Giordana, M.T., Piccinini, M., Grifoni, S., De Marco, G., Vercellino, M., Magistrello, M., Pellerino, A., Buccinna, B., Lupino, E. and Rinaudo, M.T. (2010) TDP-43 redistribution is

an early event in sporadic amyotrophic lateral sclerosis. *Brain Pathol.*, **20**, 351–360.
42. Neumann, M., Sampathu, D.M., Kwong, L.K., Truax, A.C., Micsenyi, M.C., Chou, T.T., Bruce, J., Schuck, T., Grossman, M., Clark, C.M. *et al.* (2006) Ubiquitinated TDP-43 in frontotemporal lobar degeneration and amyotrophic lateral sclerosis. *Science*, **314**, 130–133.
43. Winton, M.J., Igaz, L.M., Wong, M.M., Kwong, L.K., Trojanowski, J.Q. and Lee, V.M. (2008) Disturbance of nuclear and cytoplasmic TAR DNA-binding protein (TDP-43) induces disease-like redistribution, sequestration, and aggregate formation. *J. Biol. Chem.*, **283**, 13302–13309.
44. Winton, M.J., Van Deerlin, V.M., Kwong, L.K., Yuan, W., Wood, E.M., Yu, C.E., Schellenberg, G.D., Rademakers, R., Caselli, R., Karydas, A. *et al.* (2008) A90V TDP-43 variant results in the aberrant localization of TDP-43 in vitro. *FEBS Lett.*, **582**, 2252–2256.
45. Dormann, D. and Haass, C. (2011) TDP-43 and FUS: a nuclear affair. *Trends Neurosci.*, **34**, 339–348.
46. Kyttala, A., Lahtinen, U., Braulke, T. and Hofmann, S.L. (2006) Functional biology of the neuronal ceroid lipofuscinoses (NCL) proteins. *Biochim. Biophys. Acta*, **1762**, 920–933.
47. Auteri, J.S., Okada, A., Bochaki, V. and Dice, J.F. (1983) Regulation of intracellular protein degradation in IMR-90 human diploid fibroblasts. *J. Cell. Physiol.*, **115**, 167–174.
48. Tolkatchev, D., Malik, S., Vinogradova, A., Wang, P., Chen, Z., Xu, P., Bennett, H.P., Bateman, A. and Ni, F. (2008) Structure dissection of human progranulin identifies well-folded granulin/epithelin modules with unique functional activities. *Protein Sci.*, **17**, 711–724.
49. Sampathu, D.M., Neumann, M., Kwong, L.K., Chou, T.T., Micsenyi, M., Truax, A., Bruce, J., Grossman, M., Trojanowski, J.Q. and Lee, V.M. (2006) Pathological heterogeneity of frontotemporal lobar degeneration with ubiquitin-positive inclusions delineated by ubiquitin immunohistochemistry and novel monoclonal antibodies. *Am. J. Pathol.*, **169**, 1343–1352.
50. Le Ber, I. (2013) Genetics of frontotemporal lobar degeneration: an up-date and diagnosis algorithm. *Rev. Neurol.*, **169**, 811–819.
51. Seelaar, H., Rohrer, J.D., Pijnenburg, Y.A., Fox, N.C. and van Swieten, J.C. (2011) Clinical, genetic and pathological heterogeneity of frontotemporal dementia: a review. *J. Neurol. Neurosurg. Psychiatry*, **82**, 476–486.
52. Tanaka, Y., Suzuki, G., Matsuwaki, T., Hosokawa, M., Serrano, G., Beach, T.G., Yamanouchi, K., Hasegawa, M. and Nishihara, M. (2017) Progranulin regulates lysosomal function and biogenesis through acidification of lysosomes. *Hum. Mol. Genet.*, **26**, 969–988.
53. Beel, S., Moisse, M., Damme, M., De Muynck, L., Robberecht, W., Van Den Bosch, L., Saftig, P. and Van Damme, P. (2017) Progranulin functions as a cathepsin D chaperone to stimulate axonal outgrowth in vivo. *Hum. Mol. Genet.*, **26**, 2850–2863.
54. Zhou, X., Paushter, D.H., Feng, T., Pardon, C.M., Mendoza, C.S. and Hu, F. (2017) Regulation of cathepsin D activity by the FTLD protein progranulin. *Acta Neuropathol.*, **134**, 151–153.
55. Ward, M.E., Chen, R., Huang, H.Y., Ludwig, C., Telpoukhovskaia, M., Taubes, A., Boudin, H., Minami, S.S., Reichert, M., Albrecht, P. *et al.* (2017) Individuals with progranulin haploinsufficiency exhibit features of neuronal ceroid lipofuscinosis. *Sci. Transl. Med.*, **9**, pii: eaah5642.
56. Kishimoto, Y., Hiraiwa, M. and O'Brien, J.S. (1992) Saposins: structure, function, distribution, and molecular genetics. *J. Lipid Res.*, **33**, 1255–1267.
57. Harzer, K., Paton, B.C., Christomanou, H., Chatelut, M., Levade, T., Hiraiwa, M. and O'Brien, J.S. (1997) Saposins (sap) A and C activate the degradation of galactosylceramide in living cells. *FEBS Lett.*, **417**, 270–274.
58. Qi, X. and Grabowski, G.A. (1998) Acid beta-glucosidase: intrinsic fluorescence and conformational changes induced by phospholipids and saposin C. *Biochemistry*, **37**, 11544–11554.
59. Sun, Y., Qi, X. and Grabowski, G.A. (2003) Saposin C is required for normal resistance of acid beta-glucosidase to proteolytic degradation. *J. Biol. Chem.*, **278**, 31918–31923.
60. Fischer, G. and Jatzkewitz, H. (1975) The activator of cerebroside sulphatase. Purification from human liver and identification as a protein. *Hoppe Seylers Z Physiol. Chem.*, **356**, 605–613.
61. Morimoto, S., Martin, B.M., Kishimoto, Y. and O'Brien, J.S. (1988) Saposin D: a sphingomyelinase activator. *Biochem. Biophys. Res. Commun.*, **156**, 403–410.
62. Spiegel, R., Bach, G., Sury, V., Mengistu, G., Meidan, B., Shalev, S., Shneor, Y., Mandel, H. and Zeigler, M. (2005) A mutation in the saposin A coding region of the prosaposin gene in an infant presenting as Krabbe disease: first report of saposin A deficiency in humans. *Mol. Genet. Metab.*, **84**, 160–166.
63. Schnabel, D., Schroder, M. and Sandhoff, K. (1991) Mutation in the sphingolipid activator protein 2 in a patient with a variant of Gaucher disease. *FEBS Lett.*, **284**, 57–59.
64. Diaz-Font, A., Cormand, B., Santamaria, R., Vilageliu, L., Grinberg, D. and Chabas, A. (2005) A mutation within the saposin D domain in a Gaucher disease patient with normal glucocerebrosidase activity. *Hum. Genet.*, **117**, 275–277.
65. Vaccaro, A.M., Motta, M., Tatti, M., Scarpa, S., Masuelli, L., Bhat, M., Vanier, M.T., Tylki-Szymanska, A. and Salvioli, R. (2010) Saposin C mutations in Gaucher disease patients resulting in lysosomal lipid accumulation, saposin C deficiency, but normal prosaposin processing and sorting. *Hum. Mol. Genet.*, **19**, 2987–2997.